Available online at www.sciencedirect.com

ScienceDirect

Procedia Engineering 2 (2010) 1155–1164

Procedia Engineering

www.elsevier.com/locate/procedia

Fatigue 2010

Thermomechanical couplings in crystalline plasticity under fatigue loading

R. Seghir [a], E. Charkaluk[a], P. Dufrénoy[a], L. Bodelot[b]

[a]*Laboratoire de Mécanique de Lille - CNRS UMR 8107, boulevard Paul Langevin, 59655 Villeneuve d'Ascq cedex, France*
[b] *Graduate Aeronautical Laboratories, California Institute of Technology, Pasadena, USA*

Received 8 March 2010; revised 11 March 2010; accepted 15 March 2010

Abstract

Polycrystalline metallic materials are made of an aggregate of grains more or less well-oriented, with respect to the loading axis, for plastic gliding. Under mechanical loading, this leads to a heterogeneous deformation at the microstructure scale. This local plasticity, linked to fatigue damage, triggers a heterogeneous thermal dissipation linked to mechanical irreversibilities. Some original experimental works enabling the simultaneous determination of thermal and strain fields, in the same area, at the microstructure scale have already been realized in the laboratory on a A316L steel [1]. Two complementary ways have now to be followed: some additional numerical treatments in order to access experimental sources of dissipation and the development of the corresponding constitutive modeling at the grain scale. This second aspect is presented in this communication and concerns the implementation in the ABAQUS FE code of a constitutive model in large deformations and in coupled crystalline thermoplasticity. Using a fictive microstructure, based on a random distribution of, crystallographic orientations, and grain sizes, it enables to compare the kinematic and thermal distributions during monotonic tests, study the heterogeneity of stored energy at grain scale and test the consistent of behavior law under cycle numerical loading. Experimental analysis and simulation of thermomechanical coupling at the grain scale, seen as the sign of local damage, could lead to the definition of new thermodynamically based fatigue criteria.

Keywords: Stored energy, thermomechanical couplings, UMAT, fatigue

1. Introduction

Crack initiation prediction is a key feature in fatigue design. In this aim, many theoretical developments were done in the last decades and this conducted to different fatigue criteria. High Cycle Fatigue (HCF) criteria are then generally stress tensor based while Low Cycle Fatigue one are often defined from strain variables [2]. A lot of works were done since many years in order to improve such approaches. In fact, an alternative way consists in considering energetic approaches based on the plastic dissipation in order to draw a link between plasticity mechanisms and crack initiation. Then, in order to establish a common approach in HCF and LCF, the link between the different parts of the energy generated by the cyclic plastic activity and the crack initiation is studied [3]. More particularly,

* Corresponding author. *E-mail address*: rian.seghir@ec-lille.fr

1877-7058
doi:10.1016/j.proeng.2010.03.125

self-heating tests are often considered in order to distinguish different dissipative regimes [4]. Even if these tests generally allow to determine the endurance limit of the considered material [5], they present some inconvenients as they are based on macroscopic measurements. For example, on forged steels, damage can be anisotropic which conducts to very different fatigue limits depending on the orientation of the specimen with respects to the loading. However, in this particular case, self-heating tests exhibit the same dissipative regime, independently from this orientation and are not able to represent the damage anisotropy [6]. Therefore, it seems interesting to consider such energy balance at the microstructure scale where the strain localization occurs in order to define, in the future, an energy based crack initiation criterion. Such an energy balance coming from full-field measurements was already conducted at a macroscopic scale [7]. Such data are necessary to validate models and, more particularly, hardening laws as recently done at the macroscopic scale by Vincent [8] for common phenomenological models. More recently, mechanical tests were conducted on a 316L austenitic stainless steel with coupled kinematical and thermal measurements [1] allowing to dispose on the strain and thermal fields simultaneously and on the same area at the grain scale. One of the main conclusion of these tests is the great local heterogeneity, at each instant, on strain fields as well as on thermal fields mainly due to microstructural effects (crystallographic orientations, grain size …). It is well known that the plasticity phenomenon at this scale is due to dislocation based deformation mechanisms and these one induce energy storage/release steps depending on the dislocation motions and structures. The objective of this paper is to confront fully coupled measurements of kinematic and thermal fields at grain scale to a first numerical approach based on dislocation based constitutive models. First, the fully coupled measurements technique is described and some results are presented. Next, the constitutive models and the thermomechanical framework are introduced, and some results of simulation under monotonic and cyclic loadings are discussed.

1.1. Experimental procedure

The experimental device and results presented in this section are taken from Bodelot's works [1]. It presents an original experimental device able to study, in the same region, deformation and thermal fields at the microstructure scale.

1.1.1. Kinematic and thermal measurements

Strain fields are obtained thanks to DIC (Digital Image Correlation) performed with CorreliLMT (developed at the "Laboratoire de Mécanique et Technologie" of Cachan in France) on images of the deforming sample covered with a speckle pattern. Details about the DIC algorithm CorreliLMT are exposed in [9]. Images are grabbed during the test thanks to a Jai CV-M4+ CCD camera featuring a 1368 x 1024 matrix of detectors, each sizing 6.45 µm × 6.45 µm. To access the microstructure scale, a high magnification is obtained using a 50 mm lens and extension tubes. The resolution of the sthenic fields is 104 µm x 104 µm while computing DIC on 16 x 16 pixels subsets of the images and the precision on strain values is 0.1%.

Temperature fields are obtained by IRT (Infrared Thermography). The sample is filmed by a focal plane array Cedip Jade III MWIR camera, whose matrix is made of 320 x 240 detectors. This camera is used with a high magnification lens leading to a spatial resolution of 30 µm x 30 µm for the temperature fields. In this study, the link between the infrared radiation received by the camera and the temperature of the object is established thanks to a blackbody through a calibration procedure applied on each detector of the camera, which give a precision of 0.03°C.

1.1.2. Principle of the coupling

Since we are interested in the microstructure scale and the microstructure is different from one face or location to the other of a flat specimen, the same area of the sample has to be observed simultaneously by both cameras while taking into account that both arrays of detectors must remain parallel to the image of the sample surface to avoid introducing any distortion in the measured fields. To achieve a fully-coupled observation of the same zone, a dichroic mirror is placed in front of the sample, making an angle of 45° with the normal to its surface. Thanks to its filtering properties, the dichroic mirror transmits the infrared radiation towards the infrared camera, located in front of the sample and reflects the rest of the radiation, including the visible radiation, to the CCD camera which is perpendicular to the normal to the sample. To perform coupled measurements a special coating was designed and applied on the sample, meeting requirements of both measuring techniques with the magnifications used. When observed by the CCD camera at high magnification, it reveals a speckle aspect covering a large range over the grey

scale. Meanwhile its emissivity remains high and uniform (close to the one of the blackbody used for calibration) when observed by the infrared camera at high magnification. While strain fields obtained by DIC are expressed in the undeformed configuration, thermal fields are those of a deforming body. The DIC displacement data allowed us to track the displacement of material points in front of the infrared array in order to express the temperature fields in the undeformed configuration. Finally the data are fully-coupled insofar as both fields correspond to the same zone, at the same time and are expressed in the undeformed configuration.

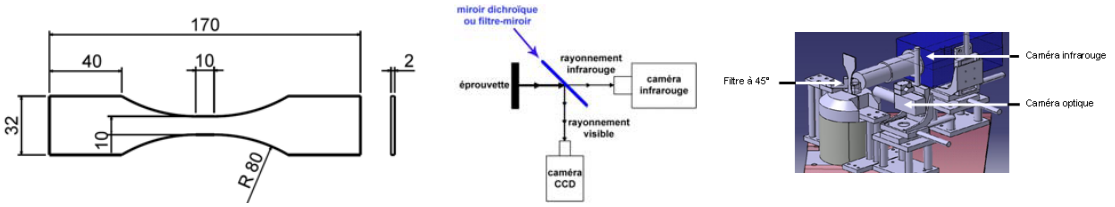

1.2. Results under monotonic tension test

As previously described, fully coupled measurements at microstructure scale were performed. Local data such as mechanical and thermal fields during monotonic and cyclic test associated to a cartography of localization of slip bands are available and constitute precious data to improve numerical model. Nevertheless, in a first step, only mean quantities and distributions during monotonic test will be introduced in this brief section.

A displacement controlled monotonic tension test with a constant strain rate of $5.10^{-3}\ s^{-1}$ has been realized. The evolution of mean stresses is presented on Figure 1 and the conventional yield stress at *0,2%* of strain is *233 MPa*. The analysis of axial deformation field shows a great heterogeneity in the observed region. On the other hand, thermal fields are more homogeneous due to the thermal diffusivity of material. It has been proved, by comparison with the observation of the microstructure after the test, that: (i) the highest deformation zones correspond to the more deformed grains, (ii) the highest temperature zones, even if they are larger due to the diffusion, could be linked to regions where the density of very deformed grains is the most significant at the end of the test [1]. In this study, we focus on mean values of fields and on their deviation in order to analyze the relative heterogeneity. The evolutions of mean strain and temperature fields and the heterogeneity of deformation and temperature are presented on figure 1.

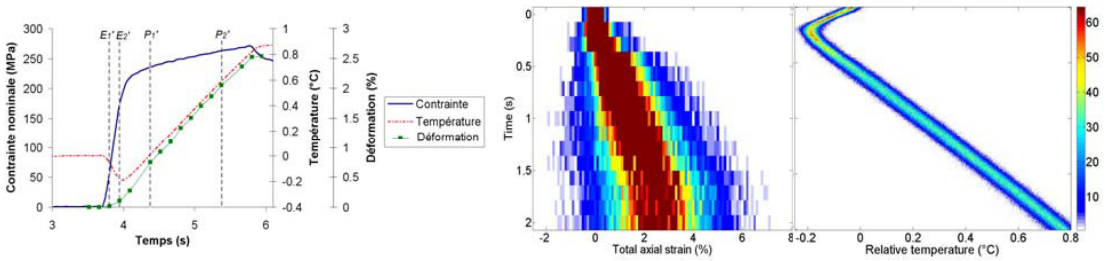

Figure 1: Average experimental results and distributions of stress, strain and temperature in A316L under monotonic tension test

We note, in a first step, a drop in temperature between points E1' and E2', both are located in conventional elastic domain, followed by a rise between points P1' et P2'. This corresponds in a first step to a thermoelastic coupling and, in a second step, to the dissipation associated to plasticity [1]. We observe that the axial deformation and temperature distribution are characterized by a Gaussian function with a significant deviation rise on deformation and that numerous grains are in contraction which is certainly due to an effect of local texture.

The objective of the numerical model, proposed in the next part, is then to be consistent with thermal and deformation measurements on mean values as well as on distribution in order to give a first estimation of local energy sources during plasticity process.

2. Finite element model

2.1. Polycristal behaviour based on dislocation densities

The elasto-visco-plastic polycrystal model assumes, in the framework of large plastic deformation and small rotation [10] an additive decomposition of the elastic and visco-plastic strain rates, D^e and D^p. This framework is used since lattice rotation plays an important role in the slip system activation. The resolved shear stress τ^s acting on a particular slip system *s* is given by the relation $\tau^s = \sigma_g^s : m^s$ where σ_g^s is the stress tensor in the grain *(g)* and m^s is the orientation tensor attributed to the slip system *(s)*: $m^s = \frac{1}{2}\left(v^s \otimes n^s + n^s \otimes v^s\right)$. n^s and v^s are the slip plane normal vector and the slip direction vector in this plane. Cubic elasticity is considered and can be described using only three parameters (C_{11}, C_{12}, C_{44}) instead plastic strain is assumed to be solely due to crystallographic dislocation flow. The resolved shear stresses on each slip system τ^s are linked to applied loading on the grain by Schmid's law and related to shear strain rate $\dot{\gamma}$ by a power law:

$$\dot{\gamma} = \dot{\gamma}_0 \left| \frac{\tau_{eff}^s}{\tau_{iso}^s} \right|^{\frac{1}{m}} sign(\tau_{eff}^s) \qquad \text{with} \qquad \tau_{eff}^s = \tau^s - \tau_{cin}^s \tag{1}$$

In this expression, τ_{iso}^s, τ_{cin}^s, $\dot{\gamma}_0$, m are respectively isotropic and kinematic variables associated to systems (s), the reference plastic strain rate and the rate sensitivity exponent. This kind of formulation was used for example in [11]. Isotropic hardening is expressed as function of dislocations density $\dot{\rho}^i$ on slip systems *i* and their interactions by means of matrix α^{ij}:

$$\tau_{iso}^s = \sqrt{\sum_u \alpha^{su} \rho^u} + \tau_0 \tag{2}$$

Where μ, b and τ_0 respectively are the shear modulus, the Burger's vector intensity and initial shear stress. For the kinematic hardening we consider here, in first approximation, a Prager's kinematic hardening [12] linearly linked with shear on slip systems:

$$\tau_{cin}^s = h v^s \tag{3}$$

Where h is the hardening modulus. Hardening flows are then governed by the evolution of dislocations density $\dot{\rho}^i$ and shear rate $\dot{\gamma}^i$.

$$v^s = \dot{\gamma}^s \tag{4}$$

$$\dot{\rho}^s = \frac{1}{b}\left(\frac{1}{L^s} - 2 y_c \rho^s\right)\left|\dot{\gamma}^s\right| \qquad \text{with} \qquad \frac{1}{L^s} = \frac{\sqrt{\sum_u a^{su} \rho^u}}{K} + \frac{1}{D} \tag{5}$$

Evolution of dislocations density is governed by an accumulation term based on Orowan's relationship and was balanced by an annihilation term which takes into account dynamic recovery during deformation. a^{su} are the

coefficients of geometrical interaction between dislocations, y_c is proportionnal to the annihilation distance of dislocation dipoles, and L^s is the average free path of mobile dislocations on the system (s) and is linked to the grain size (D). The values of the constitutive parameters described above can be obtained in the literature [13] [14] [15].

2.2. Thermodynamic framework

As introduced previously for strain rate, the free energy ψ is divided into two parts including contributions from thermo-elasticity and strain-hardening. Therefore, the Helmholtz free energy is assumed to be of the form:

$$\psi(\varepsilon^e, \theta, \alpha_i) = \psi^e(\varepsilon^e, \theta) + \psi^p(\alpha_i) \quad (6)$$

Where α_i are internal variables governing strain-hardening. According to the first and the second thermodynamical principles [16] the intrinsic dissipated power D and the thermo mechanical coupling power P_{thm} function of the free energy potential ψ are given by:

$$D = \sigma : \dot{\varepsilon}^p - \rho \frac{\partial \psi}{\partial V_i} \dot{V}_i \quad (7)$$

$$P_{thm} = \rho T \frac{\partial \psi}{\partial T \partial V_i} \dot{V}_i \quad (8)$$

Where V_i is a vector composed by all the hardening variables α_i, $\rho \frac{\partial \psi}{\partial \varepsilon^e}$ and T the temperature. In our case V_i is composed by isotropic variable p and kinematic variable α. Therefore 7 and 8 could be written as:

$$D = \sigma : \dot{\varepsilon}^p - R\dot{p} - X\dot{\alpha} \quad (9)$$

$$P_{thm} = T \frac{\partial \sigma}{\partial T} : \dot{\varepsilon}^e \quad (10)$$

Where: $R = \rho \frac{\partial \psi}{\partial p}$ and $X = \rho \frac{\partial \psi}{\partial \alpha}$. The components $\frac{\partial^2 \psi}{\partial T \partial p} : \dot{p}$ and $\frac{\partial^2 \psi}{\partial T \partial \alpha} : \dot{\alpha}$ are neglected in the thermomechanical coupling power since there are linked to phase transformation which no occurs during monotonic or cycle tests at room temperature. Dissipated power is the difference between dissipated plastic energy and stored energies in one volumetric element, by the dislocations fields. According to this fact and by analogy with the introduced framework the intrinsic dissipation is supposed to be the following:

$$D = \sum_s \left[\tau^s \dot{\gamma}^s - \left(\tau^s_{iso} - \tau_0 \right) \dot{p}^s - \tau^s_{cin} \dot{\alpha}^s \right] \quad (11)$$

Where: $\dot{p}^s = \left| \dot{\gamma}^s \right|$, $\dot{\alpha}^s = \dot{\gamma}^s$ and s are sliding system. In a first step, the crystallographic cubic symmetry is not taken into account in the energy balance and the elastic and thermal expansionary properties of material are assume to be isotropic. In this case, with respect to the classical definition [16] the free energy potential composed by contributions from thermo-elasticity could be writing:

$$\psi^e(\varepsilon^e, \theta) = \frac{1}{\rho} \left[\frac{1}{2} \left(\lambda tr(\varepsilon^e)^2 + 2\mu tr(\varepsilon^{e^2}) \right) - (3\lambda + 2\mu) \alpha \theta tr(\varepsilon^e) \right] - \frac{C_\varepsilon}{2T_0} \theta^2 \quad (12)$$

Where α and C_ε respectively are the dilatation coefficient and the specific heat at fixed strain. Therefore the thermomechanical sources are the sum of both terms:

$$D = \sum_s \left[\tau^s - \left(\tau^s_{iso} - \tau_0\right) sign(\dot{\gamma}^s) - \tau^s_{cin}\right]\dot{\gamma}^s \quad 13$$

$$P_{thm} = -\alpha T tr(\dot{\sigma}) - 3(3\lambda + 2\mu)\alpha^2 T\dot{T} \quad 14$$

2.3. Development of a User-MATerial subroutine

The crystal plasticity constitutive theory and its associated thermodynamic frameworks are not provided as standard in any of commercially available finite element analysis software. It is therefore necessary to implement the theory in the form of a User-defined stress update algorithm. This subroutine use the finite element code ABAQUS/standard, an implicit solver, and is written in Fortran 77. It implements the model in term of stress update algorithm which is called at each integration point, for each time increment during a finite element simulation. The non linear coupled system is solved by a Newton method. This pattern introduces a non symmetric jacobian matrix:

$$\begin{pmatrix} K_{uu} & K_{\theta u} \\ K_{u\theta} & K_{\theta\theta} \end{pmatrix} \begin{Bmatrix} \Delta u \\ \Delta T \end{Bmatrix} = \begin{Bmatrix} R_u \\ R_\theta \end{Bmatrix} \quad 15$$

In a first step no fully coupled calculation is considered. In result, local variables linked to $K_{\theta u}, K_{u\theta}$ are considered as null. Therefore, at scale of integration point, Abaqus only need the calculation of $K_{uu} = \dfrac{\partial \Delta\sigma}{\partial \Delta\varepsilon}$, $K_{\theta\theta} = \dfrac{\partial RPL}{\partial \Delta T}$ (*RPL* correspond to the sum of incremental source terms (cf. 13 and 14) and σ .

In the framework of crystal plasticity, σ is determined from shear calculation. By definition, the increment of shear is:

$$\Delta\gamma^s = \dot{\gamma}_{(t+\Delta t)}\Delta t \quad 16$$

$\dot{\gamma}_{(t+\Delta t)}$ is associated to $\Delta\gamma^s$ by implicit functions of dislocation densities $(\dot{\rho}^s)$ crystal orientations (D^s, W^s) and stress (σ). Therefore a totally implicit formulation would be relatively time consuming and seems to be difficult to compute. Here, a semi implicit formulation is used. Iteration loops on variables $(\dot{\rho}^s, D^s, W^s, \sigma)$ are operated to solve the explicit equation function of $\Delta\gamma^s$ (cf. 17). This method makes the calculation converges from the explicit solution to the good one in few iterations. According to the framework and the variables introduced earlier, and using a forward gradient scheme [17] the explicit formulation of shear increment $\Delta\gamma^s$ and his validity criterion [18] give:

$$\sum_u \left[\delta^{su} + \frac{\theta\Delta t}{\tau^s_{iso(i)}} \frac{\partial \dot{\gamma}^s}{\partial X^s}\bigg|_{(i)} \left(R^s_{(i)} : D^u + X^s_{(i)} H^{su}_{(i)} sign(\gamma^u{}_{(i)}) + h_{(i)}\right) \right] \Delta\gamma^u{}_{(i)} = \dot{\gamma}^s{}_{(i)}\Delta t + \frac{\theta\Delta t}{\tau^s_{iso(i)}} \frac{\partial \dot{\gamma}^s}{\partial X^s}\bigg|_{(i)} \left(R^s_{(i)} : D\Delta t\right)$$

$$\Delta\gamma^s{}_{(i)} = \left[(1-\theta)\gamma^s{}_{(t)} + \theta\dot{\gamma}^s{}_{(i)}\right]\Delta t \quad 17$$

With *i* the number of iteration. For further details concerning numerical scheme used and the meaning of variables, we invite interested readers to refer to [19].

Finally, concerning the input and output variables, at the beginning of every iteration of analysis, ABAQUS/standard provides the subroutine with the logarithmic, strain and strain increment, $\varepsilon_{(t)}$, $\Delta\varepsilon_{(t+\Delta t)}$ within finite strain framework, temperature and temperature increment at the next increment, $T_{(t)}$, $\Delta T_{(t)}$, stress update at the lastest increment, $\Delta\sigma_{(t)}$, and state variables which correspond to all needed internal variables.

2.4. Comparison between numerical and experimental study and discussion

2.4.1. Model

A polycrystalline thermo-elasto-plasticity 3D finite-element model has then been developed, corresponding to a 316L austenitic stainless steel thin specimen. The model is, for the moment, a simplified representation of an eighth of the specimen center region, containing about 20 grains (cf. Figure 2). It represents a random heterogeneity of grain morphology and crystallographic orientation. Range of grain size and crystallographic orientation respectively are [0.2mm3, 2.5mm3] and [0°, 45°]. Apart from the grain orientations, same properties are considered in every grain and every slip direction at the beginning of the test and the model does not take into account the behaviour of grain boundaries. Finally the model is composed by about 2500 tetrahedral elements C3D8RT. In future works the model will take into account the real morphology, number, and orientation of grain using E.B.S.D analysis of specimens used in experimental investigations. It is clear that, as soon as these data will be available, this step will allow a real comparison between mechanics and thermal fields at the grain scale.

Figure 2(b) and (c) respectively present the mechanical and thermal boundary conditions and loadings. The model is composed by 3 mechanical symmetries along the 3 normal directions. These symmetries are thermally modelled by thermal flux equal to zero. The convective exchange with the air is introduced on faces 1 and 2 (cf. Figure 2(c)) and the loading is applied on face 3. Two kinds of loadings have been simulated with this E.F. model: monotonic tensile tests to compare the accuracy with significant experimental results and tension compression cyclic test to improve the constitutive law under reversed loadings.

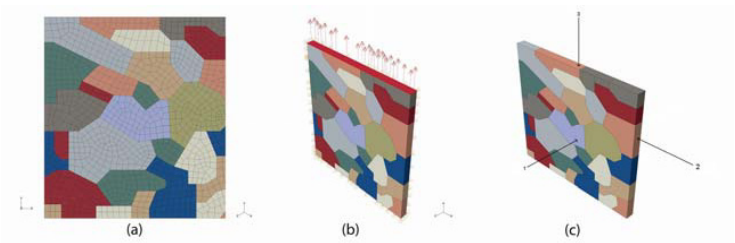

Figure 2: F.E model - (a) microstructure (b) mechanical boundary conditions (c) thermal boundary conditions

2.4.2. Monotonic tension test

A displacement controlled monotonic tensile test is simulated until 3.5% of strain with the boundary conditions previously described. Several results are compared at 2.5% of deformation which corresponds to the experimental P'^2 event. Figure 3(a) gives the mean evolution of stress, strain and temperature during the test. At *2.5%* of deformation the stress is about *265 MPa* and the difference in temperature compared to the initial value is about *0.95°C*. This is consistent with experimental results (cf. Figure 1) concerning the yield stress and hardening evolution. Nevertheless the average temperature is overestimated about 0.1°C more. This could be explain by the simplicity of boundary conditions which are, for example, adiabatic on the upper face of the model instead of taking into account for significant thermal leak through the upper grip [5] [7].

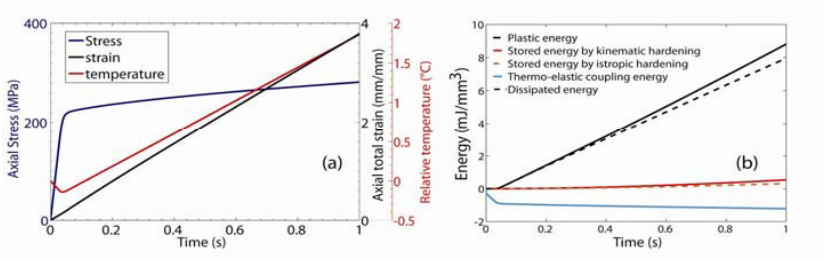

Figure 3: Average evolution of (a) stress, strain temperature and (b) energy in polycrystalline steel during monotonic tension test

Finally, the temperature is consistent with the thermo mechanical couplings: initial drop and then a rise due to plastic dissipation. Figure 3(b) introduces results concerning average deformation energy and its part stored in material by dislocation flow. Five curves are represented: the total plastic deformation energy which level is about *8.5mJ/mm*^{3} at *3.5%* of deformation, the part of this quantity which is dissipated in heat form which tend to *90%* of plastic energy (in line with the traditional assumption), the stored energy coming by isotropic and kinematic hardening, about *0.5mJ/mm*^{3}, and finally the thermo-elastic coupling, about *-1mJ/mm*^{3}. These results are, for example, in line with results of [20] even if our model seems to underestimate the stored part which conducts therefore to an overestimation of the temperature on Figure 3. Furthermore, the stored energy by kinematic hardening is more significant than energy stored by isotropic hardening. The consequence is a linear evolution of total stored energy and consequently a lack of saturation.

Moreover, the main interest of the numerical model is the possible study of the local heterogeneity which corresponds to the Figure 4(a) to (d). It gives the heterogeneity of stresses, temperatures, stored energies and deformation on the specimen face. This reveals a strong heterogeneity on the elastic domain as well as on the plastic one. More particularly, at *2.5%* of average deformation, the heterogeneity is about *290 MPa* on stress, *1.2°C* on temperature, *0.2 J/mm*^{3} on stored energy and about *2%* on strain. This behaviour is qualitatively consistent with previous results of [21] concerning aggregate calculation which are in contradiction with traditional assumption of homogeneous stress or strain at macroscopic scale.

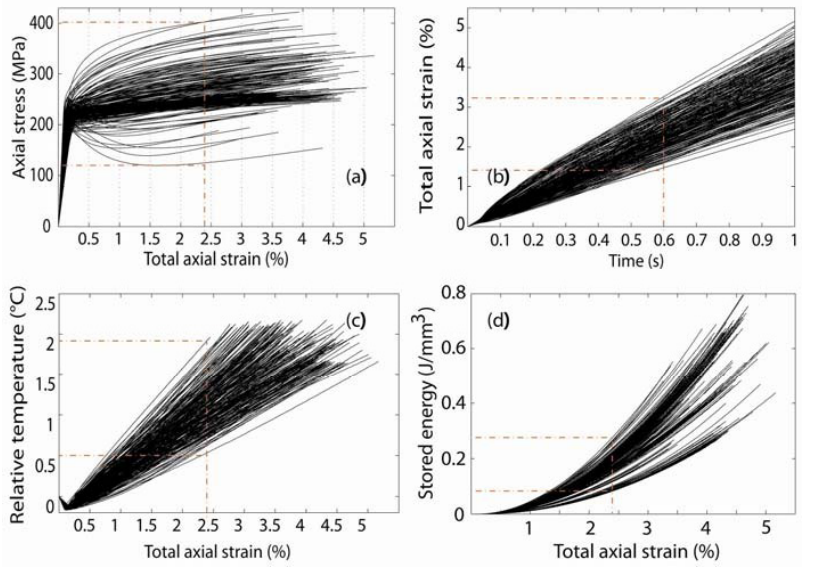

Figure 4: Local evolution of (a) stress (b) strain (c) temperature (d) stored energy in polycrystalline steel during monotonic tension test

Nevertheless, compared to the experimental results, the heterogeneity of deformation is divided by two instead heterogeneity of temperature is twice. This could be due to too simple mechanical and thermal boundary conditions.

2.4.3. Cyclic test

Similarly, a cyclic tension-compression test with a strain between [-0.6%, 0.6%], is simulated and the 20 first cycles are studied. We observe on Figure 5(a) a saturation of stress after the second cycle and a hardening until a stabilized cycle between [-320 MPa, 370 MPa]. It well exhibits the coupling between isotropic and kinematic hardening. Figure 5(b) presents the evolution of temperature variations from 0 to 16°C. It clearly shows thermo-elasto-plastic coupling phenomenon but, as previously described, because of adiabatic boundary conditions and underestimation of stored energy, the temperature rise is too important compared with experimental data [21]. Figure 5 (c), (d) and (e) present local data. The first one shows the evolution of distribution in strain which becomes more homogeneous cycles after cycles and its scatter larger in [-2%, 2%] interval after 20 cycles whereas average strain remains the same. The last one presents the maximum and minimum envelope of energy, as well as the average, stored by isotropic (d) and kinematic (e) hardening. It first shows a great heterogeneity in both cases. Contrary to the monotonic test, the model shows that the isotropic hardening is more significant in the storage of energy under low cycle fatigue than under monotonic test. Nevertheless, note that this result is closely linked to kinematic hardening flow which is in our case very simple.

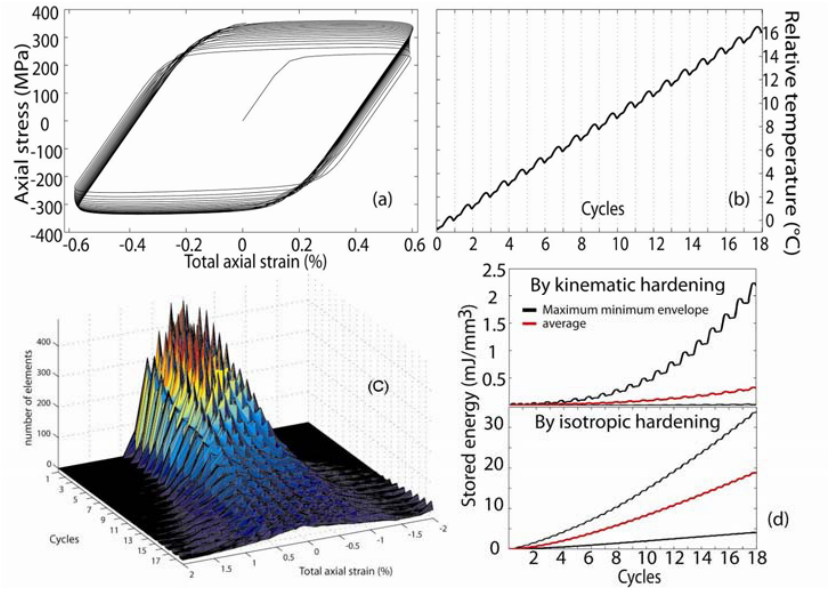

Figure 5: Evolution of average and local quantities in polycrystal during cycles of loading: (a) Evolution of average stress function of average strain (b) evolution of average temperature (c) evolution of strain distribution strain (d) evolution of stored energy by kinematic hardening and (e) by isotropic hardening

The interest of such simulations is to be able to link the stored energy quantities to physical variables as dislocations densities. The important question is the link between energy storage and localization process and after, to damage initiation. One of the difficulties here is the great dependence of the results to the chosen model and its parameters [8]. The next step of this work is therefore to focus on the hardening laws definition, with a particular attention to production/annihilation processes and temporary energy storage.

3. Conclusion

Original experimental works enabling the simultaneous determination of thermal and strain fields, in the same area, at the microstructure scale and experimental results under monotonic tension test has been presented. An F.E

model based on constitutive theory of dislocation density under large deformation was introduced. It enables thermomechanical simulation tests under monotonic and cyclic loading. Results in both kinds of loadings are presented and exhibit a very important heterogeneity of strain, stress, temperature and stored energy at microstructure scale. In future works, this framework allows us to study the interaction between local constitutive law and stored quantities, between stored quantities and localisation of damage. An E.B.S.D mapping of experimental specimen is under progress and will be introduced in the model with experimental mechanical and thermal boundary conditions. It will enable a real comparison of thermal and mechanical fields and will provide a more quantitative analysis of local results.

References

[1] Bodelot, L., Sabatier, L., Charkaluk, E. and Dufrénoy P." Experimental set up for fully-coupled kinematic and thermal measurements at the microstructure scale of an AISI 316L steel " Mat. Sci. Eng. A, 501:52-60, 2009.
[2] Socie D. F. et Marquis G. B. "Multiaxial fatigue." SAE Inc Warrendale, 2000
[3] E. Charkaluk and A. Constantinescu. Dissipative aspects in High Cycle Fatigue. Mech. Mat., 41 :483–494, 2009
[4] Luong M. P. "Infrared thermographic scanning of fatigue in metals." Nuclear Engineering and Design, 1995, 158, 2-3, pp. 363-376
[5] Doudard C, Calloch S, Hild F, Cugy P, Galtier A: Identification of the scatter in high cycle fatigue from temperature measurements. Comptes Rendus Mecanique 2004, 332:795-801.
[6] Pessard E: Comportement anisotrope en fatigue des composants mécaniques forgés. PhD thesis. Université d'Angers; 2009 (in french)
[7] Boulanger, T., (2004) " Analyse par thermographie infrarouge des sources de chaleur induites par la fatigue des aciers ", Thèse de doctorat de l'université de Montpellier II, Spécialité Mécanique (in French).
[8] Vincent L. "On the ability of some cyclic plasticity models to predict the evolution of stored energy in a type 304L stainless steel" high cycle fatigue. European Journal of Mechanics - A/Solids, 27, 2, pp. 161-180, 2008.
[9] Hild F, Raka B, Baudequin M, Roux S, Cantelaube F. Multiscale displacement field measurements of compressed mineral-wool samples by digital image correlation. Applied optics. 2002 10 November 2002;41(32):6815-28.
[10] Lubliner, J., 1990. Plasticity Theory. Macmillan.
[11] Saai, A., 2007. Physical model of FCC single crystal behaviour under alternated loading: contribution to the definition of multiscale modeling of metals forming processes. Ph.D. Thesis, Université de Savoie (in French).
[12] Prager, W., 1956. A new method of analyzing stresses and strains in work-hardening plastic solids. Journal of Applied Mechanics ASME 23, 493-496.
[13] Eriau, P., Rey, C. "Modeling of deformation and rotation bands and of deformation induced grain boundaries in IF steel aggregate during large plane strain compression",. International Journal of Plasticity 20 (2004) 1763-1788.
[14] Evrard, P., Aubin, V., Degallaix, S. and Kondo, D. "Formulation of a new single crystal law for modeling the cyclic softening",.Mechanics Research Communications 35 (2008) 589- 594.
[15] Libert, M. (2007) "Etudes experimentale et numérique de l'effet des mécabnismes de plasticité sur la rupture fragile par clivage dans les aciers faiblement alliés",.Ph.D. Thesis, Ecole Centrale de Paris (in French).
[16] Lemaitre J. et Chaboche J.-L. "Mécanique des Matériaux Solides." Bordas, 1988.
[17] Peirce, D., Shih, C. F. and Needleman, A., 1984."A tangent Modulus Method for Rate Dependent Solids",. Computers & Structures, .v.18, p.875.
[18] Huang, Y. (1991) "A User-MATerial subroutine incorating single crystal plasticty in the ABAQUS finite element program",.Division of applied sciences Harvard University, Cambridge, MA 02138
[19] Harewood, F.J.and McHugh, P.E., Comparaison of the implicit and explicit finite elemnt methods using crystal plasticity. Computational Materials Science 39 (2007) 481-494.
[20] Chrysochoos A., Maisonneuve O., Martin G., Caumon H. et Chezeaux J. C. ´n Plastic and dissipated work and stored energy. ´z Nuclear Engineering and Design, 114, 3, pp. 323-333, 1989.
[21] Forest,.S., Cailletaud, G., Jeulin, D., Feyel, F., Galliet, I., Mounoury, V.,Quilici , S., "Introduction au calcul de microstructures Elements of microstructural mechanics", Mécanique & Industries 3 (2002) 439-456
[22] Bodelot L: Étude couplée des champs cinématiques et thermiques à l'échelle de la microstructure des matériaux métalliques. PhD thesis. Université des Sciences et Technologie de Lille - Lille I; 2008 (in french)